POLITECNICO DI TORINO
Repository ISTITUZIONALE

A novel method of assessing and predicting coated cutting tool wear during Inconel DA 718 turning

(Article begins on next page)

29 November 2022

A novel method of assessing and predicting coated cutting tool wear during Inconel DA 718 turning

S. Capasso[a], J.M. Paiva[b,e,*], E. Locks Junior[b], L. Settineri[c], K. Yamamoto[d], F.L. Amorim[e], R.D. Torres[e], D. Covelli[f], G. Fox-Rabinovich[b], S. Veldhuis[b]

[a] *Department of Mechanical Engineering, Politecnico Di Torino University, Torino, 10129, Italy*
[b] *McMaster Manufacturing Research Institute, McMaster University, Hamilton, L8SL7, Canada*
[c] *Department of Management and Production Engineering, Politecnico Di Torino University, Torino, 10129, Italy*
[d] *Kobe Steel Ltd, Kobe, 652271, Japan*
[e] *Mechanical Engineering Graduate Program – PPGEM, Pontificia Universidade Catolica do Paraná, Curitiba, 80215901, Brazil*
[f] *Saskatchewan Structural Sciences Centre, University of Saskatchewan, S7N 5C9, Canada*

ARTICLE INFO

ABSTRACT

This work investigates the wear characteristics of two different coating systems deposited on cemented carbide tools and used in the finish turning of an Inconel DA718 aerospace alloy. The two coatings were: (a) a new nanocomposite multilayer Ti25Al65Cr10 N/Ti20Al52Cr22Si8N PVD coating, and (b) an AlTiN benchmark coating. Four different cutting speeds (60, 80, 100 and 120 m/min) were employed during this study. Wear behavior was characterized using three-dimensional volumetric wear progression, as well as flank wear progression, wear mechanism evaluation, and cutting force analysis. A tool life predictive model was created for this process based on both 3D and flank wear patterns. The tool with the nanocomposite coating outperformed the AlTiN benchmark coating under higher speed conditions, and both tools performed best under a surface speed of 80 m/min. The primary wear mechanisms responsible for the performance of these coatings differ in relation to the adaptive behavior of the nanocomposite coating. In addition, tool wear predictions modeled under different cutting conditions demonstrated an estimated accuracy of 93%.

1. Introduction

The aerospace industry demands materials that can be used in complex environments characterized by creep and oxidation of the metal due to high temperatures. Metallic alloys such as titanium and nickel-based heat-resistant superalloys (HRSAs) are the main group of recommended materials, since they are capable of retaining their mechanical and chemical properties at elevated temperatures [1,2]. Inconel 718, an HRSA, possesses many additional advantages such as high toughness, thermal fatigue, corrosion and oxidation resistance [3]. These characteristics make Inconel 718 an attractive component for turbine engine discs, blades, and drive-shaft components used in the aircraft industry. However, this alloy is also known to be a difficult-to-machine material [4,5]. One of the major issues during the cutting process of this alloy is built-up edge (BUE) formation and high cutting temperatures generated at the cutting zone, due to the natural response of its high strain hardening, low thermal conductivity and presence of abrasive particles in its microstructure. These characteristics promote tool material chemical affinity between the cutting tool and the workpiece material. The resulting thermal stresses at the cutting tool cause rapid

tool wear, with predominant wear modes being flank, notch, crater wear, plastic deformation, and chipping [5–10].

In light of this, adequate tool selection is needed. Current literature considers tool geometry, material, surface engineering, coatings, and different cutting conditions [4,10–15] as solutions to the high machining costs of Inconel 718. The most significant improvement of Inconel 718 machining thus far was achieved by tool surface engineering using Physical Vapor Deposited (PVD) coatings [16]. PVD coatings have particular characteristics such as enhanced mechanical properties, reduced friction coefficient and thermal conditions that favorably affect cutting performance and consequently, the tool life, which has a direct impact on machining costs and product quality [17].

However, the challenge still remains to reduce the machining costs and to produce a machined workpiece with excellent surface integrity (better surface roughness and low levels of residual stresses) even after the tool wear criterion has been reached [4,18,19]. Moreover, the surface quality of machined parts will always remain a priority for heat resistant super alloys, particularly in the aerospace industry [18,20]. One method suggested in Refs. [6,18,21,22] is tool wear monitoring under real industrial conditions to evaluate surface quality (residual stresses)

on the workpiece surface generated at different stages of tool wear. Other studies suggest increasing the cutting speed to increase chip flow, thereby obtaining better surface integrity on the machined workpiece [20]. Higher cutting speeds raise temperatures in the cutting zone, which reduces workpiece mechanical properties and tool life [19,23].

Literature describes the effects of several PVD coatings during the machining of HRSAs. Results show improvement in tool life and surface integrity due to the PVD coatings possessing a number of beneficial characteristics such as high corrosion resistance, high hardness, high thermal and chemical stability and good surface quality [24–31]. Previously published data on PVD nanocomposite coatings shows that they perform better than conventional PVD coatings [31]. Therefore, to increase the productivity and quality of machined parts in aerospace industry applications, a better understanding of the machining process is needed (in terms of cutting conditions, tooling, and the combination of the cutting tool-machine tool-workpiece). Addressing these operating conditions necessitates tool wear monitoring and prediction of the latest PVD nanocomposite coatings.

To achieve this goal, a predictive tool flank wear model based on experimental data obtained from several tests at different cutting speeds was developed in this study for the machining of nickel-based superalloys. The outcome of this model was compared with indicators such as the material removal rate (MRR), the tool wear rate (TWR) and the index of performance (IP) to obtain a comprehensive overview of the turning process. Furthermore, since optical microscope observations revealed that the primary tool wear modes were chipping and BUE, more thorough wear analyses were needed. An innovative investigation into the three-dimensional tool wear progression assesses the extent by which hard PVD nanocomposite coatings can protect the carbide substrate.

2. Experimental procedure

2.1. Coating system

The coatings proposed in this research are an AlTiN PVD coating and a multi-layered TiAlCrN/TiCrAl52Si8N PVD nanocomposite coating. The AlTiN is commercially available from Kennametal. This coating was selected as the benchmark since it is widely used in industry due to its superior tool life and maximum cutting speed, especially under finishing cutting conditions. Meanwhile, the multi-layered TiAlCrN/TiCrAl52Si8N nanocomposite coating has been deposited on the carbide substrate using SFC (Super Fine Cathode) physical vapor deposition. The multi-layered Ti0.25Al0.65Cr0.1 N/Ti0.2Al0.52Cr0.22Si0.08 N coating was deposited on a cemented carbide tool WC-Co substrate in a R&D-type hybrid PVD coater (AIPSS002, Kobe Steel Ltd.) using a plasma-enhanced arc source. The Ti0.2Al0.52Cr0.22Si0.08 and Ti0.25Al0.65Cr0.1 produced by a powder

metallurgical process were used to deposit the nanocomposite multi-layered coating. Prior to the deposition of the nanocomposite coating, the samples were heated up to about 500 °C and cleaned through an Ar ion etching process. Next, N_2 mixture gas was fed to the chamber at a pressure of 4 Pa. The arc source was operated at 150 A for a 100 mm diameter x 16 mm thick targets. The other deposition parameters were bias voltage 150 V and substrate rotation 5 rpm. The typical coating thickness, for the deposition parameters mentioned above, was around 2 μm. All the coatings were deposited on cemented carbide grade K313 cutting inserts provided by Kennametal. This cemented carbide grade consists of hard low binder containing unalloyed WC/Co fine grain with 6% Cobalt. Cemented carbide hardness and density are respectively 93 HRA and 14.9 g/cm^3. CNGG cutting insert geometry and its dimensions are presented in Fig. 1.

The microstructural and phase transformation at the cutting tool/workpiece interface as well as the chemical composition of the formed tribo-films was studied with X-ray photoelectron spectroscopy (XPS) on a Kratos Analytical Inc. (Manchester, UK) AXIS Supra spectrometer equipped with a hemispherical energy analyzer and an Al anode source for X-ray generation. A monochromatic Al K-α X-ray (1486.6 eV) source was operated at 15 kV. The system base pressure was no higher than 1.0×10^{-9} Torr with an operating pressure that did not exceed 2.0×10^{-8} Torr. Before any spectra were collected from them, the samples were sputter-cleaned for 4 min using a 4 kV Ar + beam. A 110 μm beam was used for all the data collected from the samples. Pass energy of 160 eV was used to obtain all survey spectra while pass energy of 40 eV was used to collect high-resolution data. All spectra were obtained at a 90° takeoff angle and Kratos' charge compensation ensured neutralization of all samples. Data was calibrated using a C1s signal of C-C at 284.8 eV. All data analysis was performed using Casa XPS version 2.3.18PR1.0 software.

The mechanical properties of the coating systems were measured with a Hysitron Tribo-Indenter TI-900. For this test, a diamond probe tip Berkovich model was selected alongside a 500 mN load. The hardness and elastic modulus of the coating systems were measured through 16 indentations distributed in a 4 × 4 matrix over a top polished coating. The hardness results and elastic modulus were obtained from the indentation load-unloading curves according to the Oliver and Pharr method [32]. Moreover, to evaluate the adhesion strength of the coating system, a CSM Instrument Revetest - Scratch tester was employed. The experiments were carried out according to the ASTM C1624 standard. Scratch tests were conducted under a progressive load from 5 to 200 N in a Rockwell C model indenter over a 3 mm length at a speed of 6 mm/min. Finally, previous studies [33,34] show the procedure adopted in this work to evaluate the chemical composition, thickness
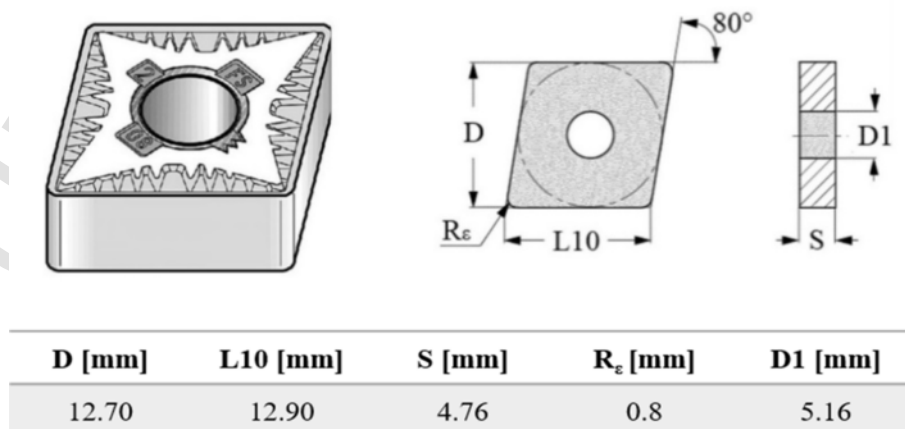

D [mm]	L10 [mm]	S [mm]	R$_\varepsilon$ [mm]	D1 [mm]
12.70	12.90	4.76	0.8	5.16

Fig. 1. Geometry of the tools ISO CNGG120408FS.

and cross-section morphology of the coatings using a Transmission Electron Microscope (TEM).

2.2. Workpiece material and cutting tests

The workpiece material tested in this research was a heat resistant nickel-based superalloy Inconel 718. The Inconel 718 workpiece material was a cylinder with a diameter and height of 76.2 mm and 250 mm, respectively. The Inconel 718 was heat treated and aged according to the AMS 5662 standard, resulting in a hardness around 40 HRC. Its microstructure, chemical composition and mechanical properties are presented in Fig. 2.

The cutting tests were performed on an Okuma Crown L1060 CNC lathe. Cutting inserts were fixed in a standard tool holder (Kennametal - ISO designation PCLNL 2525 M16). The tool holder geometry is as follows: back rake angle, $\lambda 0 = -5$; clearance angle, $\alpha 0 = 5°$; cutting edge angle, $\beta 0 = 90°$; rake angle, $y0 = -5°$; side cutting edge angle, $\chi r = 95$.

Cutting tests were performed under wet conditions at four different cutting speeds ($V_c = 60; 80; 100; 120 \ m/min$) for both coated tools. All other cutting parameters (depth of the cut $d = 0.25mm$, and a feed rate of $f = 0.1225mm/rev$ were kept constant throughout the experiments. A semi synthetic oil fluid with 6% concentration was used as a coolant at a flow rate of 20 L/min. For each of the cutting conditions listed above, a set of three trials were performed. Flank wear was measured for each trial according to an ISO 3685 standard using a Keyence VHX 5000 digital microscope. The failure criterion was flank wear of 300 μm.

To evaluate coated tool machining performance, flank wear (VB) versus cutting length (L) was determined for each cutting speed investigated in this project. The cutting length can be expressed as:

$$L = \sum l_i = \sum \frac{\pi D_i * l_{1_i}}{1000f} \tag{1}$$

where L is the total length of the cut, l_i is the cutting length for each pass (considering an average tool life of $1000m$, a reasonable cutting length of $130m$ was chosen for each step to adequately approximate the tool life curve without introducing excessive discontinuity), D_i represents the diameter of the workpiece in millimetres, l_{1_i} is the linear length (mm) of the machined workpiece during a pass and f is the feed rate in millimetres per revolution. Tool wear and surface roughness

were measured after each pass. Surface finish was measured from an average of 3 values acquired by a Mitutoyo SJ-201 portable profilometer. To ensure the reliability of the results, the portable roughness device was calibrated using a high-accuracy Mitutoyo Formtracer Extreme CS-5000 profilometer and Flexbar Machine Corporation certified standard roughness samples. During the surface roughness measurement, the cut off length was kept at 0.8 mm and evaluation length at 4 mm.

Furthermore, to understand the tribological conditions on the cutting zone, a study of the chip undersurface roughness and chip formation (chip compression ratio, shear angle, friction angle, shear strain, ship sliding velocity, chip flow angle, cutting force, and friction coefficient at the tool-chip interface) were carried out by standard methods [36,37]. Chips were collected after a machined length of 130 m during the cutting tests.

2.3. Assessment and quantification of progressive tool wear

A fundamental part of this study is the comparison of 3D volume wear and built-up edge evolution during the tool life tests for the proposed coated tools. A focus variation microscope (FVM), model Infinite Focus G5 by Alicona was used to perform these studies. Each unworn corner was evaluated by FVM prior to the machining process to obtain a comparison dataset for 3D volume wear evaluation and to estimate the built-up edge amount after each cutting test pass. This procedure was also validated in other studies [38]. 3D frames scanned from the cutting tools with Alicona FVM underwent post-processing, as shown in Fig. 3. To assess the evolution of cutting tool wear, a 3D image was aligned and compared with the previous pass shape and the fresh corner shape after each cutting pass, as shown in Fig. 3.

The parameters extracted from this process with Measure Suite software are presented in Table 1.

3. Results and discussion

The cross-section SEM micrographs of TiAlCrN/TiCrAl52Si8N and AlTiN PVD coatings, presented in Fig. 4a indicates that AlTiN coatings have a columnar structure. In contrast, the TiAlCrN/TiCrAl52Si8N coating presented in Fig. 4b has a multilayer architecture combined with a columnar structure of the entire coating layer. Multilayer coatings exhibit a common tendency to refine the columnar structure [40]

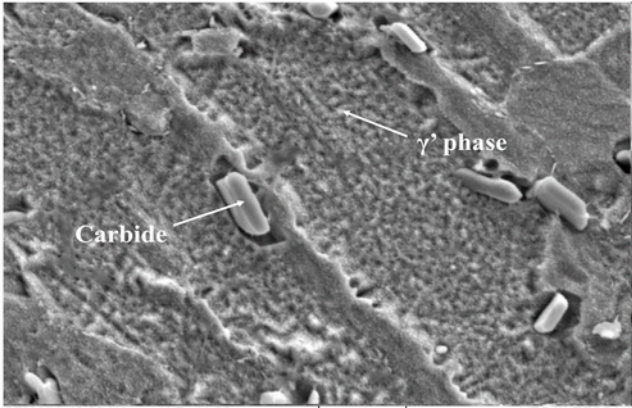| Element	Weight %	Yield Strength [MPa]	Tensile Strength [MPa]	Elongation %	Hardness [HB]
Ni	50÷55	1034	1275	12	331
Mn	<0.35				
P	<0.015				
S	<0.015				
Si	<0.35				
Cr	17÷21				
C	<0.08				
Mo	2.80÷3.30				
Nb	4.75÷5.50				
Ta	<0.05				
Ti	0.65÷1.15				
Al	0.20÷0.80				
Co	<1.00				
B	<0.006				
Cu	<0.15				
Fe	Bal.				

Fig. 2. Chemical composition, mechanical properties and SEM of the microstructure of Inconel DA718 obtained at room temperature.

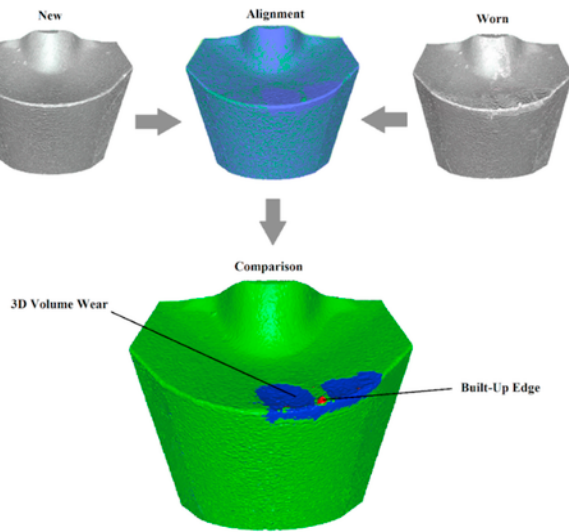**Fig. 3.** A graphical explanation of post-process analysis.

Table 1
Data extracted from the 3D analysis.

Peak Volume	Vp [μm³]	Volume of material exceeding the reference surface of the original insert.	BUE
Valley Volume	Vv [μm³]	Volume of material below the reference surface of the original insert.	3D Wear
Incremental Peak Volume	Vp_discr [μm³]	Volume of material exceeding the reference surface delimited by the previous pass.	BUE
Incremental Valley Volume	Vv_discr [μm³]	Volume of material below the reference surface delimited by the previous pass.	3D Wear

Furthermore, the worn tools were also evaluated by a scanning electron microscope (SEM), model Tescan Vega II LSU SEM to assess the wear on worn tools evaluated by FVM.
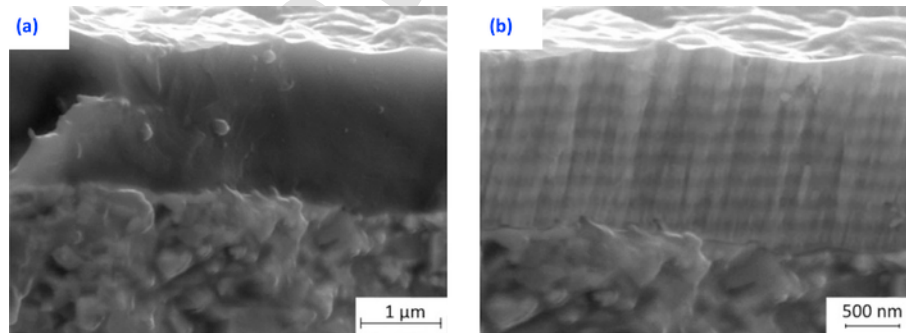
as shown in Fig. 4b. Therefore, outstanding wear resistance could be achieved, resulting in longer tool life service.

The mechanical properties (hardness, reduced elastic modulus, H^3/E_r^2 ratio, and adhesion strength) of the two coatings are summarized in Table 2. The hardness of the TiAlCrN/TiCrAl52Si8N nanocomposite coating is 38 GPa, being slightly higher than that of the monolayer Al-TiN PVD coating (around 35 GPa). Table 2 features the chemical composition of the coatings in addition to the H^3/E_r^2 ratio. The elastic modulus of the nanocomposite coating is also higher than that of AlTiN. In fact, the loading support of the nano-composite coating (H^3/E_r^2 ratio) is higher than that of AlTiN, which is beneficial for the heavy loaded conditions present in Inconel machining [35,39]. Although the multilayer TiAlCrN/TiCrAl52Si8N nanocomposite coating is slightly thicker than the AlTiN PVD coating, this coating system shows better adhesion to the substrate (Lc2) as shown in Table 2.

Moreover, the structure of the nano-composite coatings was studied using XPS. Fig. 5 shows the XPS results obtained from the coated sample. The data obtained through XPS on the surface of the coating at the initial state, indicates the presence of a Si_3N_4 phase, which is an amorphous phase in this family of coatings [41].

Fig. 6 shows the behavior of tool flank wear as a function of the cutting at the following cutting speeds: 60 m/min, 80 m/min, 100 m/min and 120 m/min. Moreover, at the given cutting speeds, the nanocomposite performs better than the monolayer coatings. At high cutting speeds, (100 and 120 m/min) both PVD coating systems featured high flank wear and a reduced tool life. This is because high cutting speed generates more heat within the cutting zone which is quickly dissipated throughout the workpiece and the cutting tool, accelerating wear.

The advantage of using the nanocomposite coating at speeds of 60 m/min and 80 m/min is that it increases tool life (Fig. 6). Moreover, at a cutting speed of 80 m/min, wear progression is almost linear, whereas at 60 m/min, the steady-state wear region was the longest.

Based on different cutting speeds and tool life curves, the tool wear rate (TWR) was calculated from the relation between the total tool wear *(VB_B)* and total machined cutting length *(l)* as presented in equation (2).

$$TWR = \frac{VB_B}{l} \left[\frac{\mu m}{m} \right] \tag{2}$$

Fig. 4. SEM micrographs showing the cross-sections of coated samples: (a) monolayer AlTiN PVD and (b) multilayer TiAlCrN/TiCrAl52Si8N PVD coating obtained by AIP – SFC system.

Table 2
TiAlCrN/TiCrAl52Si8N and AlTiN coatings mechanical properties and characteristics.

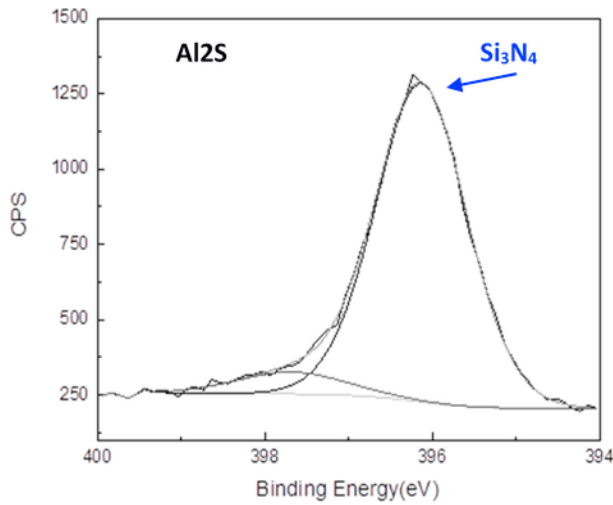| Coating	Chemical composition (EDS data)	Layer	Hardness [GPa]	Thickness [μm]	Reduced Elastic Modulus [GPa]	H^3/E_r^2	Critical Load Lc_2 [N]
TiAlCrN/TiCrAl52Si8N	Ti0.25Al0.65Cr0.1 N/ Ti0.2Al0.52Cr0.22Si0.08 N	Multi-Layer	38	2	517	0.205	124
AlTiN	Al66Ti34 N	Mono-Layer	35	1.8	497	0.173	108

Fig. 5. XPS data on the initial surface of the nanocomposite coating obtained by the AIP – SFC system.

The material removal rate (MRR) and the index of performance (IP) were obtained to represent the efficiency of the machining process:

$$MRR = d * f * V_C * 1000 \left[\frac{mm^3}{min}\right] \tag{3}$$

$$IP = \frac{MRR}{1000 * TWR} \left[\frac{m^3}{min}\right] \tag{4}$$

where *(d) is the diameter of the current cut; (f) is the feed rate and (Vc) is the cutting speed.* Thus, the productivity parameters were determined for both coatings under different cutting speeds.

Since the material removal rate (MRR) was evaluated in mm^3 per minute, it serves as a constant indicator for both coatings under the same cutting speed, as shown in Table 3.

Tool life results obtained with TiAlCrN/TiCrAl52Si8N reveal that at a cutting speed of 80 m/min, productivity increases. At this speed, the TWR is lowest and IP highest out all tested conditions (Table 3). Even compared to the lower cutting speed (60 m/min), the tool life of TiAlCrN/TiCrAl52Si8N was extended to 80 m/min, implying a potential productivity advantage.

IP average values clearly indicate that a higher TWR impairs in high production time and cost. In both tested coating systems, the average tool wear rate is about 50% higher at the highest cutting speed (120 m/min) than the lowest (60 m/min). Considering this, previous results ob-
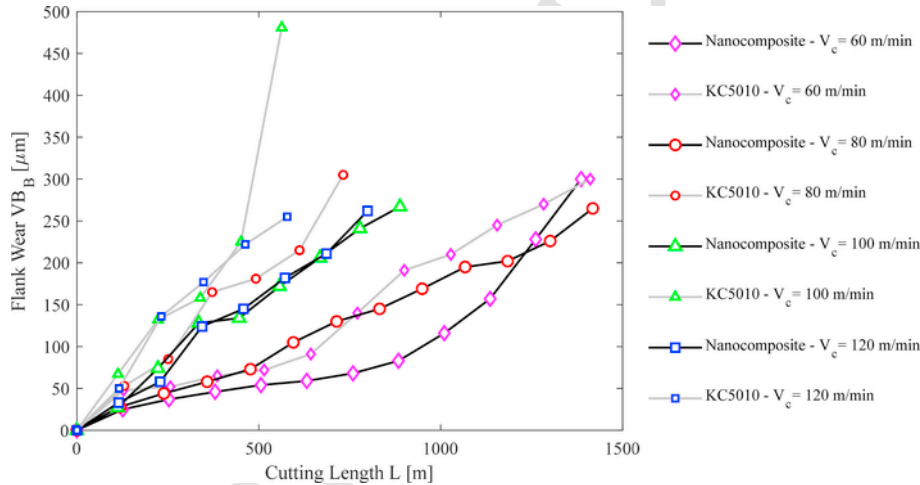

Fig. 6. Tool life curve comparison between AlTiN PVD and TiAlCrN/TiCrAl52Si8N at different cutting speeds.

Table 3
Comparison of performance indicators between the nanocomposite coating and AlTiN PVD at different cutting speeds.

		Speed (m/min)			
Coating	Parameter	60	80	100	120
Nano-composite	TWR (μm/m)	0.22 ± 0.0018	0.190 ± 0.0015	0.3 ± 0.0015	0.33 ± 0.0013
	Length (m)	1386	1418	888	799
	IP (m³/min)	8.35	12.89	9.90	11.14
AlTiN - KC5010	TWR (μm/m)	0.21 ± 0.0016	0.42 ± 0.0016	0.9 ± 0.0014	0.44 ± 0.0012
	Length (m)	1411	732	536	578
	IP (m³/min)	8.75	5.83	3.30	8.35
MRR (mm³/min)		1838	2450	2971	3675

tained with TiAlCrN/TiCrAl52Si8N demonstrated an improvement of 30% in terms of IP. From this point of view, results obtained at different cutting speeds indicate that productivity is improved the most at a cutting speed of 80 m/min. Furthermore, the nanocomposite coating's effect is more pronounced at higher cutting speeds (IPs are significantly higher than in the benchmark KC5010), as the temperature is high enough to activate the formation of protective tribofilms and spinodal decomposition [42], which provides protection to the cutting tool rake surface.

Therefore, the tool wear behavior and IP of both coatings under cutting speeds of 80 and 120 m/min will be the subject of detailed investigation in this work. The goal is to develop a system of estimating tool wear under real cutting conditions present in aerospace component machining.

According to the previously listed experimental procedure, a progressive 3D tool wear measurement of cutting tools was performed during the cutting tests at speeds of 80 and 120 m/min. Tool surface profiles were evaluated and compared with an unworn cutting tool. Typical 3D surface images of the analyzed tools were obtained at 130 m, 600 m and at the end of each tool's life. The surface images are presented in Fig. 7. The peaks and valleys on the surface are visible in both coated tools tested at different speeds.

The behavior of the two coating systems was different at the low speed of the first pass. A small amount of build-up edge (BUE) was present on the nanocomposite coating after a cutting length of 130 m, whereas BUE was the main mode of tool wear in the KC5010 coating. After a length of cut of around 600 m, the surface damage (valleys) of the KC5010 coating was higher than that of the nanocomposite. The opposite behavior can be observed at the higher cutting speeds. As is very well known, the formation of BUE during cutting is an unstable process that causes cracks, chipping and substrate exposure, all of which may result in catastrophic failure. At a low speed, the nanocomposite coating exhibited less tool wear (Fig. 7).

At a high cutting speed during the initial stage of wear, intensive BUE forms on KC5010 but not on the nanocomposite coating. However, after a cutting length of 600 m, the nanocomposite coating undergoes significant chipping due to the formation of an unstable BUE (Fig. 7).

In order to understand the wear behavior and wear mechanisms between the different coatings systems, Fig. 8 shows optical images comparing the tool wear morphology obtained for both coating systems at the same cutting length, which corresponds to the end of the tool life for AlTiN PVD coating. These studies provide a detailed investigation of the tool wear patterns that emerge during cutting, with comparison of both coating systems side by side. At low and high cutting speeds, the major wear mechanism found for both systems is adhesion followed by oxidation and abrasion wear (Fig. 8a and b). Normally, Inconel machining is characterized by intensive work hardening and elevated cutting temperatures. These two factors promote oxidation and abrasion wear mechanisms. As such, these two wear mechanisms emerge during the machining of Inconel, resulting in an unstable attrition wear mode. This wear mode usually develops adhesive bonds at the coated tool rake face and the workpiece material interface, generating an intense build-up-edge (BUE). Moreover, the coated cutting tool cannot sustain elevated loads during cutting. Eventually the tool material will flake off, leading to chipping, substrate exposure and a catastrophic failure of the cutting tool. This is the predominant wear mode in the AlTiN coated tool. (Fig. 8a and b). Conversely, BUE intensity is improved in the nanocomposite coating (Fig. 8a and b). One of the main characteristics of this coating is its ability to reduce buildup formation and intensity of tool surface damage. Tool wear images (Fig. 8a and b) confirm that the nanocomposite coating improves the friction conditions on the tool/chip interface. This coating is also capable of sustaining heavy loads at high temperatures by producing thermal barrier tribo-oxides, which reduce friction at the chip/tool interface. Clearly, only plastic deformation associated with abrasion and minor adhesion wear could be found in this coating system (Fig. 8a and b). Therefore, the tool wear patterns confirm the characteristics of adhesive wear during Inconel DA 718 machining at both speeds (80 and 120 m/min).

XPS data presented in Fig. 9 shows that in addition to sapphire tribo-films, a noticeable amount of mullite tribo-films form with enhanced thermal barrier properties (Fig. 9a) [39]. This results in im-
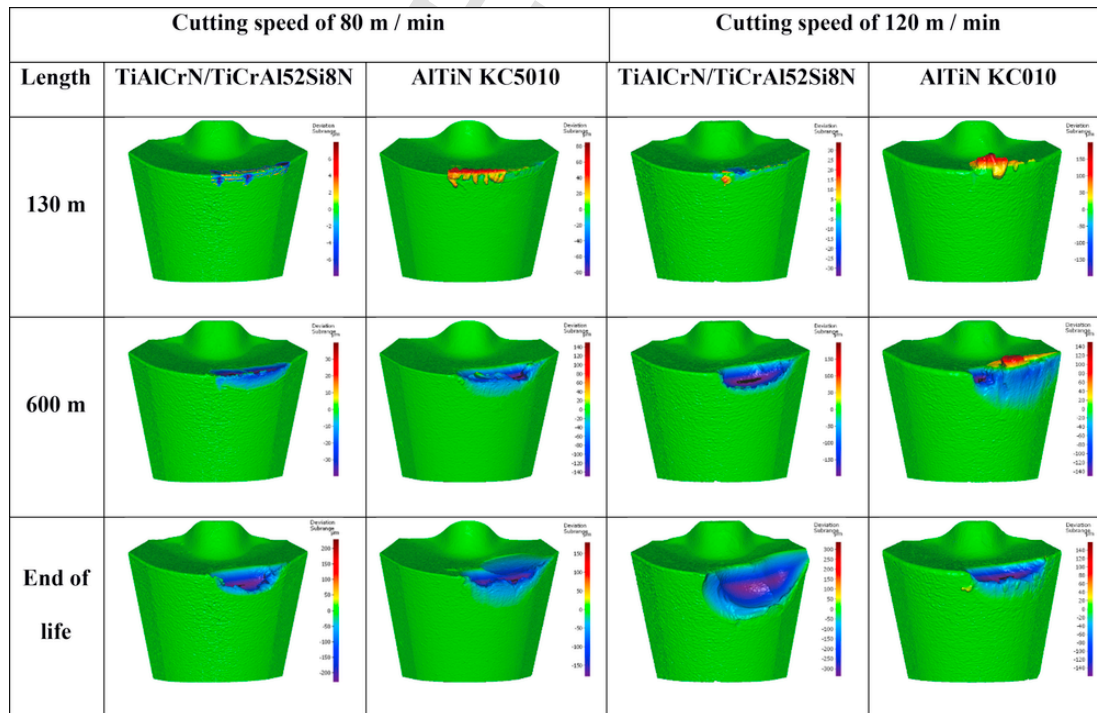

Cutting speed of 80 m / min		Cutting speed of 120 m / min	
Length	**TiAlCrN/TiCrAl52Si8N**	**AlTiN KC5010**	**TiAlCrN/TiCrAl52Si8N**	**AlTiN KC010**
130 m				
600 m				
End of life				

Fig. 7. 3D progressive tool wear for AlTiN PVD and TiAlCrN/TiCrAl52Si8N obtained in different cut lengths: 130 m, 600 m and end of the tool life during machining of Inconel DA718 at low and high cutting speeds.
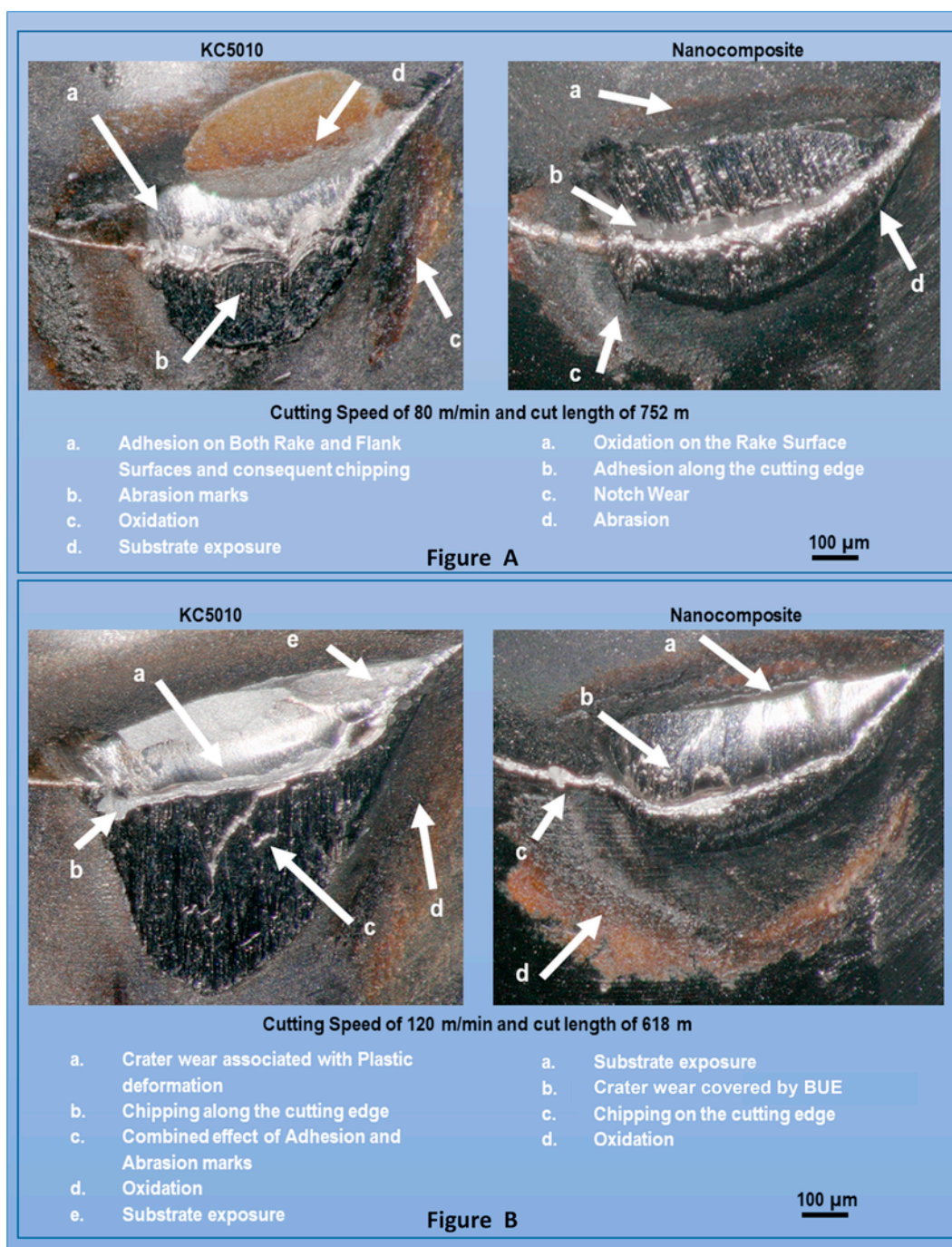
Fig. 8. Optical images comparing the tool wear morphology obtained for both coating systems at the same cutting length which corresponds to the end of tool life in the AlTiN PVD coating: Figure A- Cutting speed of 80 m/min and Figure B – Cutting speed of 120 m/min.

proved surface protection and better wear behavior of the nanocomposite coating compared with the crystalline AlTiN PVD coating (KC 5010), which forms only a similar amount of sapphire tribo-films (Figure, 9b). It should be remarked that existing literature only emphasizes the mechanical properties of nano-composite coatings [43]. However, the data presented above shows that the nanocomposite coating features improved adaptive performance as well.

Following tool life tests, the cutting edge shows intensive accumulation of workpiece material (Fig. 7), which results in poor chip flow and high mechanical loads on the cutting edge. The combination of high loads and poor chip flow results in poor machined surface roughness. To evaluate the effect of tool wear progression, surface morphol-

ogy (S_a) was measured during the cutting tests for both tools at both selected cutting speeds. Fig. 10a shows the average of each measurement performed at 130 m, 600 m and at the end of each tested coating's tool life while Fig. 10b shows the surface topography at the end of the tool life for each condition.

According to data presented in Fig. 10a, surface roughness progresses alongside tool wear in both coatings. As cutting speed increases, the cutting tool rapidly moves around the workpiece, which combined with the tool wear condition, results in surface deterioration and contributes to irregular surface roughness (Fig. 10b). Similarly, high cutting speeds promote the accumulation of heat at the cutting zone, which intensifies tool wear and negatively impacts surface roughness.
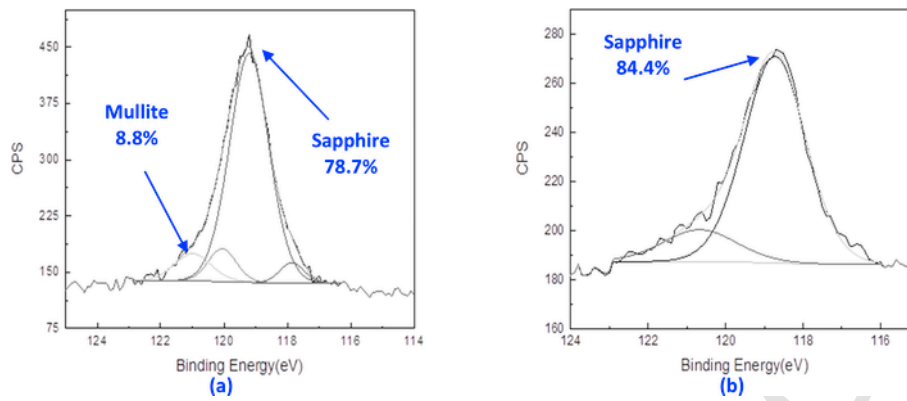
Fig. 9. XPS data on the worn surface of the a) nano-composite TiAlCrSi8N/TiAlCrN multilayer coating; b) nano-crystalline AlTiN coating.

Therefore, surfaces obtained at higher cutting speeds possess poor quality, demonstrating that cutting speed has a major impact on surface finish parameters during the machining of Inconel DA718.

Tool wear and friction in the cutting zone combined with cutting conditions are the most critical parameters affecting surface roughness during machining. To understand the tribological effects at the tool-workpiece interface, all cutting test forces were measured to yield the friction coefficient and specific cutting energy [36]. A general comparison of the cutting condition effects with tool wear, cutting forces, friction coefficient and specific cutting energy for both coatings is shown in Fig. 11. These results clearly indicate that the cutting force is governed by cutting conditions as well as tool state (Fig. 11a). The resultant increase of the friction coefficient and specific cutting energy (Fig. 11b), leads to poor surface roughness of the machined workpiece (Fig. 10). Moreover, Fig. 11c shows that the natural tool-chip contact length is influenced by the tribological conditions on the cutting zone, the cutting speeds as well as the mechanical/physical properties of the workpiece material and the coating. Under all tested conditions, the nanocomposite coating has a small contact length that decreases the tool wear and increases the IP, especially at a cutting speed of 80 m/min (Table 3).

Fig. 12 confirms that there is a good correlation between cutting speed and chip formation for both coatings tested in this work. It is also possible to see that the chips formed by the cutting tools coated with nanocomposite coatings are more curled at high and low speeds than the chips obtained with KC5010. The SEM chip undersurface images therefore confirm that KC5010 produces severe sticking of the chip to the tool rake surface at a low speed, indicating that the metal flow in this area is considerably irregular and influenced by extreme friction at the tool/chip interface. This validates that contact length (Fig. 11c) and chip curl are governed by cutting speed fluctuation, which increases the temperature at the tool-chip contact zone, altering the cutting zone tribological conditions [44].

At this point, the tribological conditions generated by a combination of different cutting speeds and coatings, play an essential role during the chip formation process for both coatings tested in this work. To understand the role of contact friction behavior at the cutting zone, a study of the tribological characteristics of the shearing work material was conducted [36]. Chips were collected at the beginning of cut (around 5 m of cutting length) and the results of chip thickness, chip compression ratio, shear angle, friction angle, shear strain, chip sliding velocity and chip flow angle were evaluated and presented in Table 4.

This data indicates significant improvement in cutting zone friction conditions during machining with nanocomposite coatings. All obtained figures show that the chip characteristics were enhanced in the nanocomposite coating, compared to KC5010. Since less plastic deformation produces a thicker chip (CCR closer to 1), CCR values show that machining is improved with the use of nanocomposite coatings. Another critical point observed is that the sliding velocity increased along

with the cutting speed at both cutting speeds, which is a natural response. However, even at a low speed, the nanocomposite produces an accelerated metal flow process, represented by the rate index of utilization (chip sliding velocity/cutting speed) of approximately 94%. This indicator is established by the elevated IP obtained with the nanocomposite coating at the same cutting speed (Table 3). Therefore, all these characteristics confirm that the nanocomposite coating reduces friction and cutting forces (Fig. 11), leading to an overall improvement in tool life (Fig. 6).

Considering the extensive group of data obtained from the experimental procedure and to predict the relationship between tool wear and productivity, flank wear data were fitted with a three-dimensional surface, according to the general equation:

$$VB_B = a_1 + a_2 * L^{a_3} * V_c^{a_4} \qquad (5)$$

where: a_1, a_2, a_3, and a_4 are general coefficients inherent to the equation, L is the cutting length, and V_c is the cutting speed.

Fig. 13 exhibits the model surface flank wear results. This model portrays the turning of Inconel DA718 using a TiAlCrN/TiCrAl52Si8N nanocomposite coating at different cutting speeds under finish operations. It is worth mentioning that the R-square for the fitting procedure is higher than 93%, confirming the reliability of the study. Fig. 13 represents the result of the modelling.

Therefore, the resulting equation for the predictive model of the nanocomposite carbide insert coating during Inconel DA718 hard turning under finishing cutting conditions is:

$$VB_B = 0.3383 + 4.245 * 10^{-4} * L^{0.9811} * V_c^{1.414} \qquad (6)$$

This equation confirms that the multi-layered nanocomposite coating possesses advantages in the hard machining of Inconel DA 718 (Fig. 13). The most optimal cutting speed (80 m/min) was selected, along with 3D volume wear, to confirm that this new method can serve as an adequate alternative to flank wear ISO methodology for investigating tool degradation.

In Fig. 14, the 3D volume wear for both studied systems is plotted. There are two curves per coating: one represents 3D volume wear evolution with respect to the original unworn corner V_v and the other is related to the sum of the partial values of the valleys' volume between the subsequent passes $V_{v_{discr}}$. It is worth mentioning that end of tool life is reached in both coatings when V_v is between $1.7 * 10^7$ and $2.4 * 10^7$. This can be explained by the structure of the two inserts and their degradation. Since both are formed from the same carbide substrate, the rake face likewise develops cratering once the coating becomes abraded. This provides ground for the establishment of 3D wear end of life criteria in carbide tools during Inconel DA 718 machining, regardless of the selected coating structure.

Although the difference between the incremental and absolute curves is not significant, the incremental curve gives more accurate re-
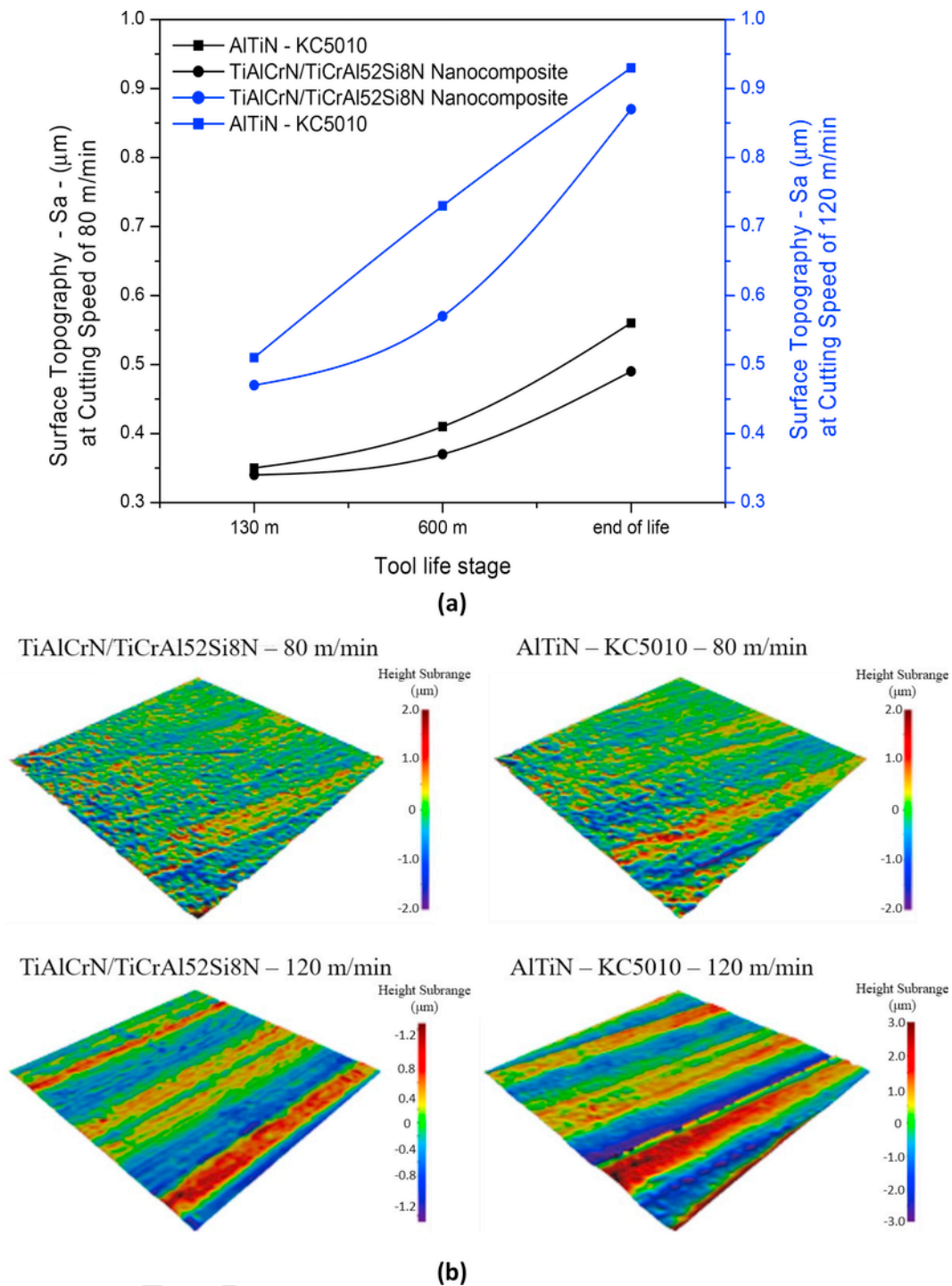
Fig. 10. Workpiece surface topography evaluation. (a) Average of surface topography measured at a different stages of tool wear and (b) Surface topography images obtained at the end of tool life for both coatings under low and high cutting speeds.

sults. To explain this, it is necessary to consider a condition in which the tool-tip reaches the end of life: in this case, there would be high 3D volume wear and an eventual BUE over the worn area that might not exceed the surface limit of the new corner. Therefore, the BUE would have a reducing effect on the measured quantity of 3D volume wear. As is shown in the graph (Fig. 14), the curves of V_v are positioned behind the curves of $\sum V_{v_{discr_i}}$, and are thus more accurate.

In Fig. 15, a comparison between the wear and 3D volume wear is plotted for both coated tools. It is worth noting that the two methods of describing the tool life show different trends. While the tool life curves

(Fig. 6) could be divided into three regions with each possessing a different trend, 3D volume wear continues to increase at a more intensive pace towards the end of life. Moreover, the growth of 3D wear is more regular than that of flank wear, which is strongly variable in a hard-to-cut material due to the limited tool life. Tracking this measure makes it possible to more accurately predict the tool life in hard turning.

As this machining process is strongly associated with build-up edge formation (Figs. 7 and 8), the build-up edge diagrams were also plotted for both KC5010 and TiAlCrN/TiCrAl52Si8N (Fig. 16). To express this quantity, the values of V_p were ignored in favor of incremental val-
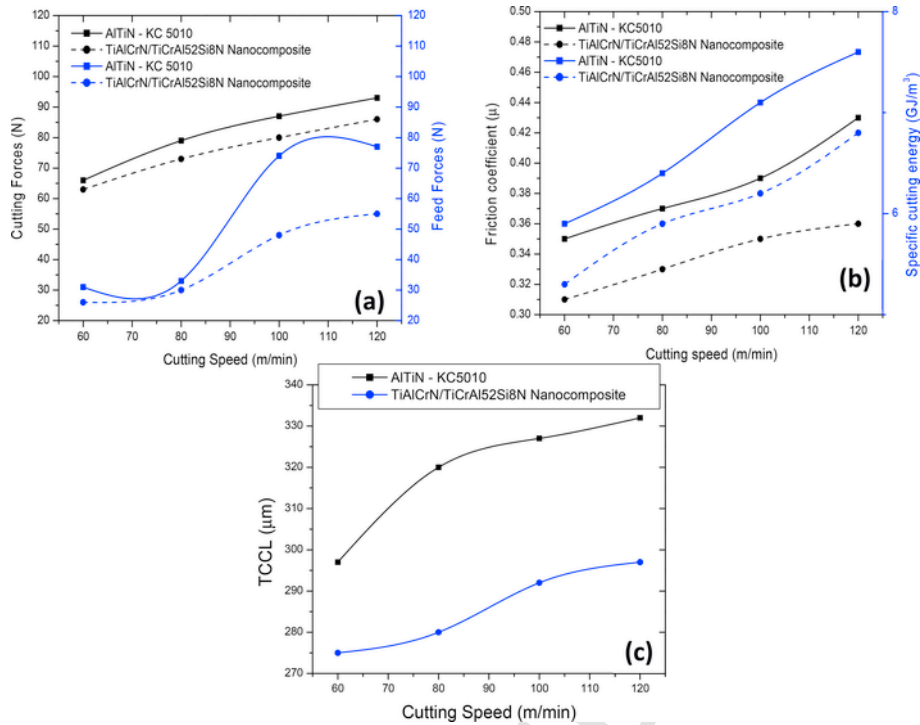
Fig. 11. Tribological conditions in the cutting zone obtained at the end of tool life for both coatings under different cutting conditions: cutting and feed forces (a), friction coefficient and specific cutting energy (b) and the tool-chip contact length (c).
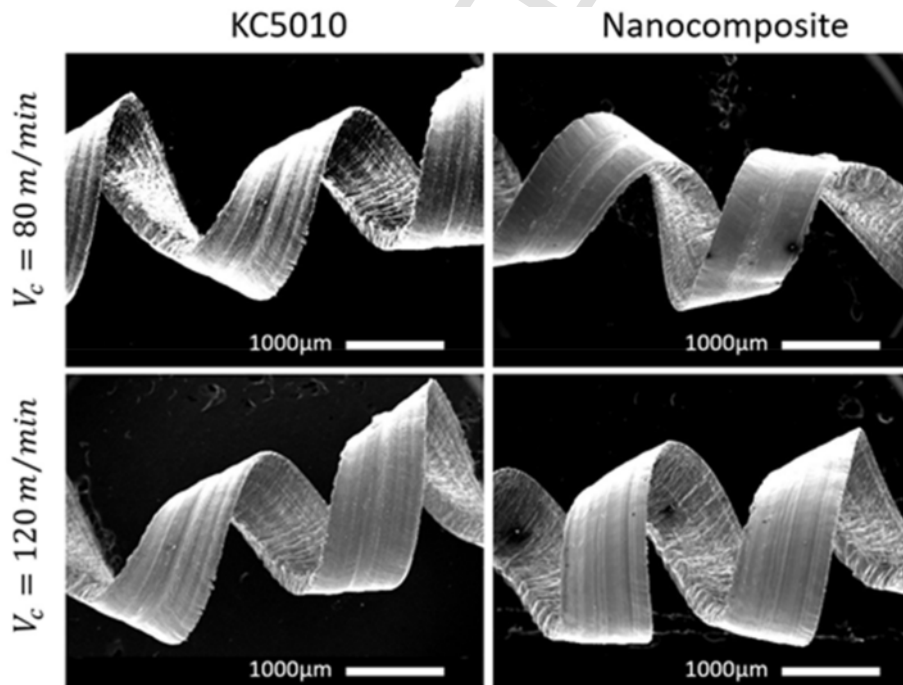

Fig. 12. SEM images of the chip undersurface obtained with KC5010 and TiAlCrN/TiCrAl52Si8N during machining of Inconel DA718 at a low and high cutting speed.

ues between subsequent passes $V_{p_{discr}}$ and their sum $\sum V_{p_{discri}}$. BUE evolution is an unstable phenomenon consisting of continuous material adhesion from the workpiece that consequently detaches and carries off a part of the tool body. Tracking BUE progression on the unworn tool tip surface could filter out this effect because it would disregard the amount of material already attached and detached during the previous passes. This measure is in any case an approximation, since BUE is not tracked instant-by-instant and evaluating the real modification is not possible with available technologies.

BUE instability is demonstrated in Fig. 16 through the increment of peak volume in relation to the previous pass. Therefore, the sum of $V_{p_{discr}}$ highlights the difference between the total amount of adhered material in the KC5010 tool and the nanocomposite one. In addition, the end of life cutting length was considerably longer (approximately $1400m$) in the nanocomposite than in KC5010 (about $700m$). Almost twice the material adhered on the benchmark coating: this confirms
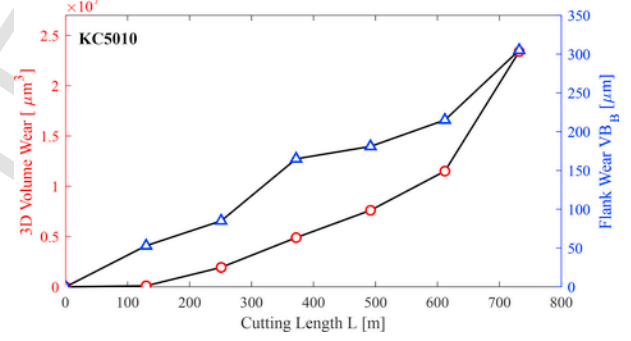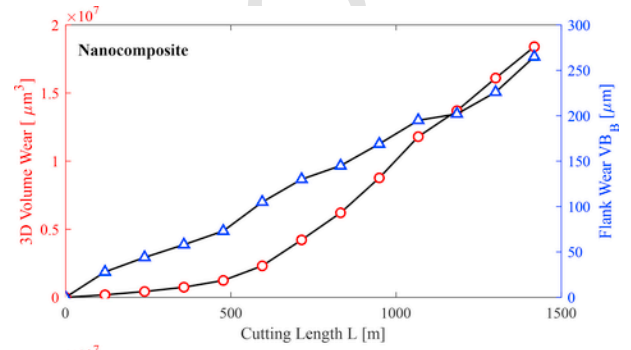
Table 4

Results of chip characteristic studies (chip thickness, chip compression ratio, shear angle, friction angle, shear strain, chip sliding velocity and chip flow angle) evaluated for both coatings at different cutting speeds (80 and 120 m/min).
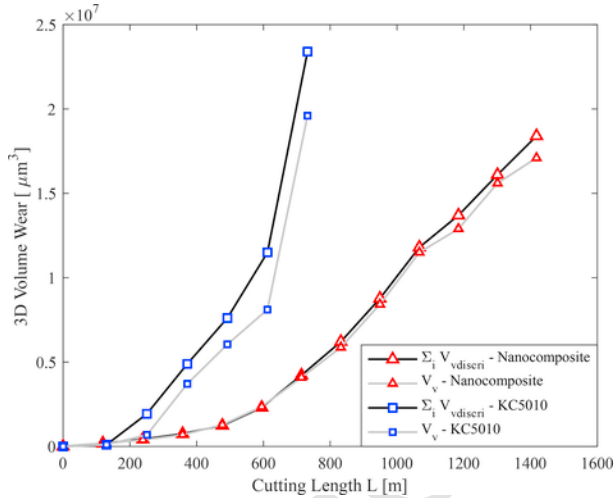
Coating	Cutting Speed (m/min)	Chip Thickness (mm)	Chip Compression Ratio - CCR	Φ - Shear Angle (°)	β - Friction Angle (°)	(Υ) Shear Strain	Chip sliding Velocity (m/min)	Chip flow angle (°)
KC5010	80	0.152	0.802	40.7	9.3	0.94	64.22	21.13
	120	0.173	0.705	36.82	13.7	0.97	84.64	26.15
Nanocomposite	80	0.14	0.871	43.22	8.9	0.92	77.08	27.32
	120	0.154	0.792	40.67	10.3	0.95	95.09	29.07
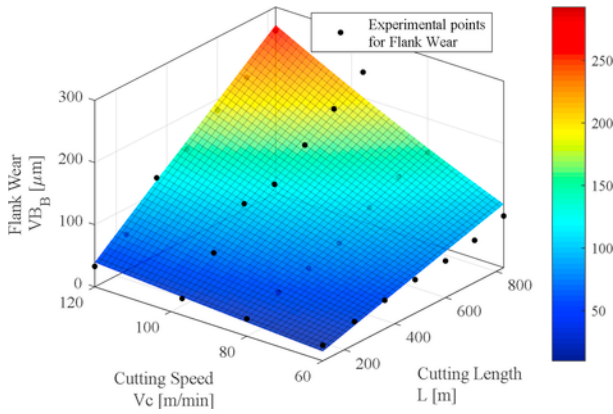
Fig. 13. Fitting of the Flank Wear experimental data predictive model for the nanocomposite coating at different cutting speeds.
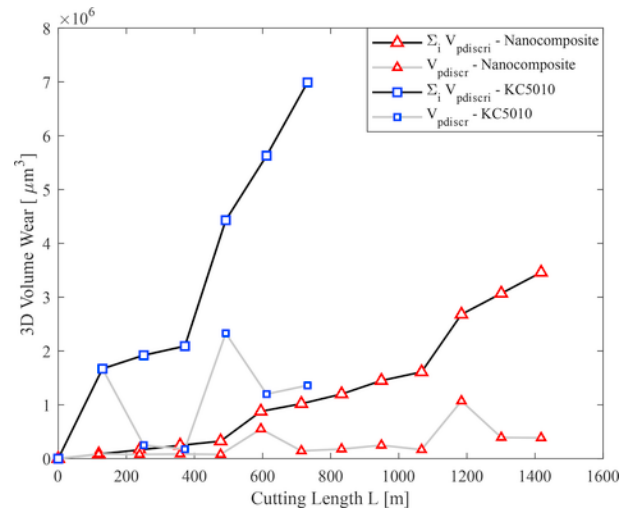

Fig. 14. 3D volume wear evolution along the tool life for KC5010 and TiAlCrN/TiCrAl52Si8N, considering both the full (V_v) and the sum of the incremental - $\sum V_{vdiscri}$

Fig. 15. Comparison between flank wear and 3D volume wear trends for the nanocomposite (left) and KC5010 (right) coatings.

Fig. 16. BUE evolution along the tool life for KC5010 and TiAlCrN/TiCrAl52Si8N, considering the incremental peak volume ($V_{p_{discr}}$) and its sum ($\sum V_{p_{discri}}$)

that the nanocomposite coating improves the lubricity and thermal protection during the cutting process.

Also, it can be seen in Fig. 13 that the 3D tool wear trends might resemble an exponential curve. As such, curve fitting performed by the Curve Fitting Matlab tool yielded interesting outcomes. The fitting is shown in Fig. 17. From the graph, it is worth noting that the 3D volume wear trends are well approximated by exponential curves, with different coefficients of the two coating structures' functions. Indeed, in both cases, the evaluated R-square is higher than 95%.

Considering a general starting exponential equation passing from the origin in the form:

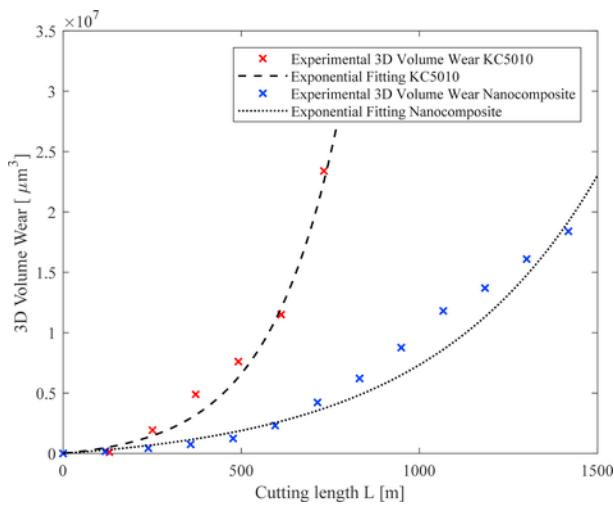$$y = a * \left(e^{bx} - 1 \right) \tag{7}$$

Fig. 17. 3D Volume Wear exponential fitting for the Nanocomposite and KC5010 coated tools.

In which y is the 3D volume wear and x is the cutting length, the coefficients a and b extracted from the fitting procedure are shown in Table 5:

From 3D wear measurements and cutting test results performed under different cutting conditions, it can be concluded that the model introduced in this work for predicting tool wear and performance is suitable for industrial Inconel 718 machining applications. Moreover, it is possible with this system to determine the effect of various cutting conditions present in Inconel DA 718 machining for any coating material deposited on cemented carbide inserts. Further trials should be conducted to establish the relation between cutting tool performance during machining of other workpiece materials under different cutting conditions. Consequently, similar methodology can be applied to assess the 3D model wear for these future applications.

4. Conclusions

This paper presents a model to predict flank wear based on experimental data obtained from several tests under different cutting conditions. This model can also provide machining productivity parameters such as MRR (metal removal rate) and IP (increased productivity). Listed experimental data present a novel system of assessing 3D tool wear evolution. In addition, the wear behavior of the two different coating systems were evaluated. The following conclusions can be drawn from the results presented in this work:

- The tool coated with the PVD nanocomposite coating outperformed the benchmark coated tool for cutting speeds greater or equal to 80 m/min. Demonstration of the fact that nanocomposite coatings feature adaptive behavior is the major scientific novelty in this study.
- During machining of Inconel DA718 the predominant wear mechanisms are adhesion followed by abrasion. The combination of these mechanisms resulted in chipping and crater wear at low and high cutting speeds.
- Nanocomposite coating design firmly modifies the wear behavior during machining of Inconel DA718 in comparison with the AlTiN PVD coating. Tool wear patterns also confirmed the characteristics of

adhesive and abrasive wear during the machining of Inconel DA 718 under both speeds (80 and 120 m/min). However, cutting tools coated with the nanocomposite coating exhibited a substantial reduction in chipping intensity, thus confirming superior wear resistance.

- Wear modes, workpiece surface finish quality evaluation, cutting forces, chip formation and coefficient of friction are primarily a function of the cutting speed and chemical composition of the coating layer during Inconel 718 DA turning.
- The flank wear prediction equation for nanocomposite coating obtained from dataset fitting demonstrated an adequate level of reliability with an R-value $\geq$ of 93%. Therefore, the applied methodology proves that the volumetric wear prediction method is more reliable than the flank wear prediction method.

Uncited references

[35].

References

[1] J.L. Cantero, J. Díaz-Álvarez, M.H. Miguélez, N.C. Marín, Analysis of tool wear patterns in finishing turning of Inconel 718, Wear 297 (2013) 885–894. https://doi.org/10.1016/j.wear.2012.11.004.

[2] R. M'Saoubi, D. Axinte, S.L. Soo, C. Nobel, H. Attia, G. Kappmeyer, S. Engin, W.-M. Sim, High performance cutting of advanced aerospace alloys and composite materials, CIRP Ann 64 (2015) 557–580. https://doi.org/10.1016/j.cirp.2015.05.002.

[3] S. Sui, J. Chen, E. Fan, H. Yang, X. Lin, W. Huang, The influence of Laves phases on the high-cycle fatigue behavior of laser additive manufactured Inconel 718, Mater. Sci. Eng. A 695 (2017) 6–13. https://doi.org/10.1016/j.msea.2017.03.098.

[4] A. Thakur, S. Gangopadhyay, State-of-the-art in surface integrity in machining of nickel-based super alloys, Int. J. Mach. Tool Manuf. 100 (2016) 25–54. https://doi.org/10.1016/j.ijmachtools.2015.10.001.

[5] J.-T. Baek, W.-S. Woo, C.-M. Lee, A study on the machining characteristics of induction and laser-induction assisted machining of AISI 1045 steel and Inconel 718, J. Manuf. Process. 34 (2018) 513–522. https://doi.org/10.1016/j.jmapro.2018.06.030.

[6] D. Ulutan, T. Ozel, Machining induced surface integrity in titanium and nickel alloys: a review, Int. J. Mach. Tool Manuf. 51 (2011) 250–280. https://doi.org/10.1016/j.ijmachtools.2010.11.003.

[7] W. Grzesik, P. Niesłony, W. Habrat, J. Sieniawski, P. Laskowski, Investigation of tool wear in the turning of Inconel 718 superalloy in terms of process performance and productivity enhancement, Tribol. Int. 118 (2018) 337–346. https://doi.org/10.1016/j.triboint.2017.10.005.

[8] S. Olovsjö, L. Nyborg, Influence of microstructure on wear behaviour of uncoated WC tools in turning of Alloy 718 and Waspaloy, Wear 282–283 (2012) 12–21. https://doi.org/10.1016/j.wear.2012.01.004.

[9] R. M'Saoubi, T. Larsson, J. Outeiro, Y. Guo, S. Suslov, C. Saldana, S. Chandrasekar, Surface integrity analysis of machined Inconel 718 over multiple length scales, CIRP Ann 61 (2012) 99–102. https://doi.org/10.1016/j.cirp.2012.03.058.

[10] E.O. Ezugwu, Key improvements in the machining of difficult-to-cut aerospace superalloys, Int. J. Mach. Tool Manuf. 45 (2005) 1353–1367. https://doi.org/10.1016/j.ijmachtools.2005.02.003.

[11] D. Zhu, X. Zhang, H. Ding, Tool wear characteristics in machining of nickel-based superalloys, Int. J. Mach. Tool Manuf. 64 (2013) 60–77. https://doi.org/10.1016/j.ijmachtools.2012.08.001.

[12] V. Bushlya, J. Zhou, J.E. Ståhl, Effect of cutting conditions on machinability of superalloy Inconel 718 during high speed turning with coated and uncoated PCBN tools, Procedia CIRP 3 (2012) 370–375. https://doi.org/10.1016/j.procir.2012.07.064.

[13] H. Tanaka, T. Sugihara, T. Enomoto, High speed machining of Inconel 718 focusing on wear behaviors of PCBN cutting tool, Procedia CIRP 46 (2016) 545–548. https://doi.org/10.1016/j.procir.2016.03.120.

[14] E.O. Ezugwu, J. Bonney, D.A. Fadare, W.F. Sales, Machining of nickel-base, Inconel 718, alloy with ceramic tools under finishing conditions with various coolant supply pressures, J. Mater. Process. Technol. 162–163 (2005) 609–614. https://doi.org/10.1016/j.jmatprotec.2005.02.144.

Table 5

Values of the coefficients a and b for the exponential curve fitting of experimental data.

Coating	a $[\mu m^3]$	b
Nanocomposite	$1.007 * 10^6$	0.002115
KC5010	$5.759 * 10^5$	0.005044

[15] A. Bhatt, H. Attia, R. Vargas, V. Thomson, Wear mechanisms of WC coated and uncoated tools in finish turning of Inconel 718, Tribol. Int. 43 (2010) 1113–1121. https://doi.org/10.1016/j.triboint.2009.12.053.

[16] G.S. Fox-Rabinovich, K. Yamamoto, M.H. Aguirre, D.G. Cahill, S.C. Veldhuis, A. Biksa, G. Dosbaeva, L.S. Shuster, Multi-functional nano-multilayered AlTiN/Cu PVD coating for machining of Inconel 718 superalloy, Surf. Coating. Technol. 204 (2010) 2465–2471. https://doi.org/10.1016/j.surfcoat.2010.01.024.

[17] G.K. Dosbaeva, S.C. Veldhuis, K. Yamamoto, D.S. Wilkinson, B.D. Beake, N. Jenkins, A. Elfizy, G.S. Fox-Rabinovich, Oxide scales formation in nano-crystalline TiAlCrSiYN PVD coatings at elevated temperature, Int. J. Refract. Metals Hard Mater. 28 (2010) 133–141. https://doi.org/10.1016/j.ijrmhm.2009.09.003.

[18] M. Salio, T. Berruti, G. De Poli, Prediction of residual stress distribution after turning in turbine disks, Int. J. Mech. Sci. 48 (2006) 976–984. https://doi.org/10.1016/j.ijmecsci.2006.03.009.

[19] R.M. Arunachalam, M.A. Mannan, A.C. Spowage, Residual stress and surface roughness when facing age hardened Inconel 718 with CBN and ceramic cutting tools, Int. J. Mach. Tool Manuf. 44 (2004) 879–887. https://doi.org/10.1016/j.ijmachtools.2004.02.016.

[20] A.R.C. Sharman, J.I. Hughes, K. Ridgway, An analysis of the residual stresses generated in Inconel 718[TM] when turning, J. Mater. Process. Technol. 173 (2006) 359–367. https://doi.org/10.1016/j.jmatprotec.2005.12.007.

[21] A. Madariaga, A. Kortabarria, E. Hormaetxe, A. Garay, P.J. Arrazola, Influence of tool wear on residual stresses when turning Inconel 718, Procedia CIRP 45 (2016) 267–270. https://doi.org/10.1016/j.procir.2016.02.359.

[22] A. Madariaga, J.A. Esnaola, E. Fernandez, P.J. Arrazola, A. Garay, F. Morel, Analysis of residual stress and work-hardened profiles on Inconel 718 when face turning with large-nose radius tools, Int. J. Adv. Manuf. Technol. 71 (2014) 1587–1598, doi:10.1007/s00170-013-5585-6.

[23] A.R.C. Sharman, J.I. Hughes, K. Ridgway, The effect of tool nose radius on surface integrity and residual stresses when turning Inconel 718[TM], J. Mater. Process. Technol. 216 (2015) 123–132. https://doi.org/10.1016/j.jmatprotec.2014.09.002.

[24] M.Z.A. Yazid, C.H. CheHaron, J.A. Ghani, G.A. Ibrahim, A.Y.M. Said, Surface integrity of Inconel 718 when finish turning with PVD coated carbide tool under MQL, Procedia Eng 19 (2011) 396–401. https://doi.org/10.1016/j.proeng.2011.11.131.

[25] S.L. Soo, S.A. Khan, D.K. Aspinwall, P. Harden, A.L. Mantle, G. Kappmeyer, D. Pearson, R. M'Saoubi, High speed turning of Inconel 718 using PVD-coated PCBN tools, CIRP Ann 65 (2016) 89–92. https://doi.org/10.1016/j.cirp.2016.04.044.

[26] M.S.I. Chowdhury, S. Chowdhury, K. Yamamoto, B.D. Beake, B. Bose, A. Elfizy, D. Cavelli, G. Dosbaeva, M. Aramesh, G.S. Fox-Rabinovich, S.C. Veldhuis, Wear behaviour of coated carbide tools during machining of Ti6Al4V aerospace alloy associated with strong built up edge formation, Surf. Coating. Technol. 313 (2017) 319–327. https://doi.org/10.1016/j.surfcoat.2017.01.115.

[27] G.S. Fox-Rabinovich, A.I. Kovalev, L.S. Shuster, Y. Bokiy, G.K. Dosbayeva, D.L. Wainstein, V.P. Mishina, On characteristic features of alloying HSS-based deformed compound powder materials with consideration for tool self-organization at cutting 2. Cutting tool friction control due to the alloying of the HSS-based deformed compound powder material, Wear 214 (1998) 279–286, doi:10.1016/s0043-1648(97)00157-9.

[28] J. Yuan, K. Yamamoto, D. Covelli, M. Tauhiduzzaman, T. Arif, I.S. Gershman, S.C. Veldhuis, G.S. Fox-Rabinovich, Tribo-films control in adaptive TiAlCrSiYN/TiAlCrN multilayer PVD coating by accelerating the initial machining condi-

tions, Surf. Coating. Technol. 294 (2016) 54–61. https://doi.org/10.1016/j.surfcoat.2016.02.041.

[29] B.D. Beake, J.L. Endrino, C. Kimpton, G.S. Fox-Rabinovich, S.C. Veldhuis, Elevated temperature repetitive micro-scratch testing of AlCrN, TiAlN and AlTiN PVD coatings, Int. J. Refract. Metals Hard Mater. 69 (2017) 215–226. https://doi.org/10.1016/j.ijrmhm.2017.08.017.

[30] V.A. Izhevskiy, L.A. Genova, J.C. Bressiani, F. Aldinger, Progress in SiAlON ceramics, J. Eur. Ceram. Soc. 20 (2000) 2275–2295. https://doi.org/10.1016/S0955-2219(00)00039-X.

[31] B.D. Beake, G.S. Fox-Rabinovich, Progress in high temperature nanomechanical testing of coatings for optimising their performance in high speed machining, Surf. Coating. Technol. 255 (2014) 102–111. https://doi.org/10.1016/j.surfcoat.2014.02.062.

[32] Q. Kan, W. Yan, G. Kang, Q. Sun, Oliver–Pharr indentation method in determining elastic moduli of shape memory alloys—a phase transformable material, J. Mech. Phys. Solids 61 (2013). https://doi.org/10.1016/j.jmps.2013.05.007.

[33] G.S. Fox-Rabinovich, B.D. Beake, K. Yamamoto, M.H. Aguirre, S.C. Veldhuis, G. Dosbaeva, A. Elfizy, A. Biksa, L.S. Shuster, Structure, properties and wear performance of nano-multilayered TiAlCrSiYN/TiAlCrN coatings during machining of Ni-based aerospace superalloys, Surf. Coating. Technol. 204 (2010) 3698–3706. https://doi.org/10.1016/j.surfcoat.2010.04.050.

[34] G.S. Fox-Rabinovich, K. Yamamoto, B.D. Beake, A.I. Kovalev, M.H. Aguirre, S.C. Veldhuis, G.K. Dosbaeva, D.L. Wainstein, A. Biksa, A. Rashkovskiy, Emergent behavior of nano-multilayered coatings during dry high-speed machining of hardened tool steels, Surf. Coating. Technol. 204 (2010) 3425–3435. https://doi.org/10.1016/j.surfcoat.2010.04.002.

[35] B.D. Beake, L. Isern, J.L. Endrino, G.S. Fox-Rabinovich, Micro-impact testing of AlTiN and TiAlCrN coatings, Wear 418–419 (2019) 102–110. https://doi.org/10.1016/j.wear.2018.11.010.

[36] M. Shaw, Metal Cutting Principles, 2°, Oxford Unversity Press, New York, 2005.

[37] E.M. Trent, P.K. Wright, Metal Cutting (2000), doi:10.1016/B978-075067069-2/50012-7.

[38] R. Danzl, F. Helmli, S. Scherer, Focus variation - a robust technology for high resolution optical 3D surface metrology, Stroj. Vestnik/Journal Mech. Eng. 57 (2011) 245–256, doi:10.5545/sv-jme.2010.175.

[39] S. Veprek, M.J.G. Veprek-Heijman, Industrial applications of superhard nanocomposite coatings, Surf. Coating. Technol. 202 (2008) 5063–5073. https://doi.org/10.1016/j.surfcoat.2008.05.038.

[40] K. Yamamoto, M. Abdoos, J.M. Paiva, P. Stolf, B. Beake, S. Rawal, G. Fox-Rabinovich, S. Veldhuis, Cutting Performance of Low Stress Thick TiAlN PVD Coatings during Machining of Compacted Graphite Cast Iron (CGI), Coatings (2018) 8, doi:10.3390/coatings8010038.

[41] C.-L. Chang, C.-S. Huang, Effect of bias voltage on microstructure, mechanical and wear properties of Al–Si–N coatings deposited by cathodic arc evaporation, Thin Solid Films 519 (2011) 4923–4927. https://doi.org/10.1016/j.tsf.2011.01.054.

[42] G. Fox-Rabinovich, J.M. Paiva, I. Gershman, M. Aramesh, D. Cavelli, K. Yamamoto, G. Dosbaeva, S. Veldhuis, Control of self-organized criticality through adaptive behavior of nano-structured thin film coatings, Entropy 18 (2016).

[43] S. Veprek, M. Jilek, Superhard and functional nanocomposites formed by self-organization in comparison with hardening of coatings by energetic ion bombardment during their deposition, Rev. Adv. Mater. Sci. 5 (2003) 6–16. http://www.ipme.ru/e-journals/RAMS/no_1503/veprek/veprek.pdf.

[44] J.M.F. de Paiva, R.D. Torres, F.L. Amorim, D. Covelli, M. Tauhiduzzaman, S. Veldhuis, G. Dosbaeva, G. Fox-Rabinovich, Frictional and wear performance of hard coatings during machining of superduplex stainless steel, Int. J. Adv. Manuf. Technol. 92 (2017) 423–432, doi:10.1007/s00170-017-0141-4.